A Slotless PM Variable Reluctance Resolver with Axial Magnetic Field

Le Sun, *Member, IEEE,* Zhejun Luo*, Student Member, IEEE,* Jun Hang*, Member, IEEE,* Shichuan Ding*, Member, IEEE,* Wei Wang*, Senior Member, IEEE*

***Abstract*— The stator-PM machine concept has been practiced on the recently proposed stator-PM variable reluctance (VR) resolver. When inheriting the simple and sturdy rotor structure of the conventional VR resolver, the novel stator-PM VR resolver provides a chance to avoid the high-frequency (HF) excitation by the unique PM back-EMF decoding solution. This paper extends this stator-PM VR resolver category with the axial magnetic field technology. The axial slotless structure makes the VR resolver compact and much smaller than the radial field prototypes. The thin and light leaf-style rotor is suitable for the super-high-speed applications, as the additional inertia due to a sensor is not welcome in those scenarios. Additionally, the printed circuit board (PCB) replaces the winding coils in the regular VR resolvers, significantly simplifying the manufacturing. The design with even and odd poles cannot share the same principle, so they are discussed separately. The prototypes with 4-X and 5-X configurations are tested in the experiment setup respectively to validate the analysis of the proposed structure. Moreover, the 4-X resolver is integrated with a permanent magnet synchronous machine (PMSM), and a motor driver with the space vector modulation (SVM) on the basis of the specific resolver decoder is built.**

***Index Terms*— Axial slotless structure, printed circuit board (PCB) winding, stator-PM machine, variable reluctance (VR) resolver.**

I. INTRODUCTION

The variable reluctance (VR) resolver has been the dominant position feedback solution for the electric powertrain and electric propulsion systems. Better than the optical encoders and magnetic encoders, the simple and sturdy rotor of the VR resolver is attractive for the harsh application fields, such as terrible vibration and centrifugal pull [1]-[3]. Additionally, the VR resolvers are much easier to manufacture than the winding rotor resolvers. These features make VR resolvers a promising candidate for the pumps, turbos and compressors. In those applications, as the rotor speed is becoming higher than before, the delicate regular position sensors cannot get with the challenging operation condition. Meanwhile, as those types of equipment are mass products in the market, the high-cost schemes are not welcome.

About the VR resolvers, the winding distribution, slot-pole configuration, and the design of rotor contours have been discussed in existing literatures [4]-[7]. The conventional resolver technologies share the same principle [8]. They have excitation (EXC) windings, sinusoidal (SIN) and cosine (COS) windings. The decoding circuit injects high-frequency (HF) voltage signal into the EXC winding, the induced current generates magnetic flux across the SIN and COS windings. With the rotor moving, the magnetic reluctances under the SIN/COS windings are varying. Hence, the induced SIN/COS feedback voltage signals are also varying accordingly. By properly designing the rotor contours, the SIN/COS feedbacks can exhibit two orthogonal sinusoidal signals, corresponding to the rotor angular position.

The issue is that the frequency of the HF excitation must be much higher than the machine operation frequency (electrical frequency). As an example, for a 12-slot/5-pole-pair motor running at 60,000 r/min, the operation frequency is 5 kHz. To have an acceptable or adequate measurement accuracy, the excitation frequency should be at least 50 kHz. A higher operation frequency will require even Mega Hz excitation frequency. A possible solution using an inductive rotary sensor is proposed in [9], [10]. This type of sensor has the similar operation principle of the conventional VR resolvers, but the implementation requires an extremely high frequency signal injection, by special processors and integrated circuits (IC), which must increase the costs. Anyway, with a regular cost budget, this high-frequency limitation issue cannot be solved by a conventional position measurement scheme.

The stator-PM VR resolver was proposed many years ago [11]. In recent years, the stator-PM machine subject [12], [13] provides a new horizon for the related research on this exclusive resolver. The stator-PM VR resolvers share the same simple rotors structure of the common VR resolvers. As there is no need to provide electromagnetic power, only a tiny amount of magnet is required on the stator, the cost is thus friendly. Recently, paper [14]-[16] have reported this novel position sensor. As is shown in Fig.1 (a), with this concept, a 4-X prototype and the dedicated decoding setup has been developed to validate the practicability. Paper [17] proposed to mount the magnets into the stator teeth, and realized the excellent measurement accuracy by applying this stator-PM concept.

Manuscript received January 31, 2021; revised Mar 23, 2021; accepted June 2, 2021. This work was supported in part by the National Natural Science Foundation of China under Grant 51907091, in part by the Provincial Natural Science Foundation of Jiangsu province under Grant BK20190467. (*Corresponding author: Le Sun.*)

L. Sun is with the Department of Electrical Engineering, School of Automation, Nanjing University of Science and Technology, Nanjing 210094, China (e-mail: sunle@njust.edu.cn).

Z. Luo, J. Hang and S. Ding are with the School of Electrical Engineering and Automation, Anhui University, Hefei 230601, China (e-mail: luozhj@stu.ahu.edu.cn, junhang@ahu.edu.cn, dsc@ahu.edu.cn).

W. Wang is with the School of Electrical Engineering, Southeast University, Nanjing 210096, China (e-mail: wangwei1986@seu.edu.cn).

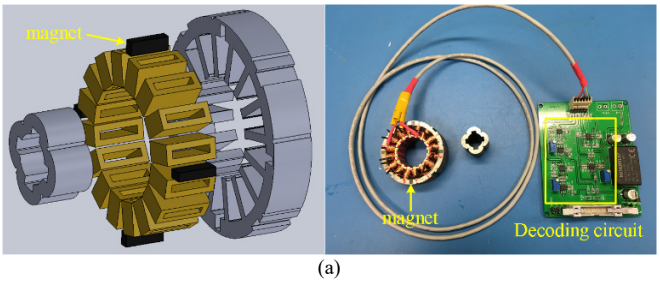

(a)

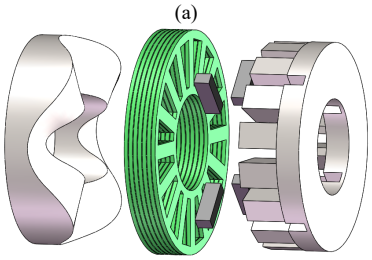

(b)

Fig. 1 The stator-PM VR resolvers. (a) A 4-X resolver prototype. (b) A concept drawing with axial structure.

The stator-PM VR resolvers have apparent advantages at the high-speed applications, as the HF excitation is not required anymore. In fact, when the machine operation frequency comes up to higher than 1 kHz, the position measurement solution will take more than a regular cost. However, in the industry, the pumps, turbos and compressors are with much higher speed than before. There are some examples, paper [18] reports a high speed machine for the compressor application (60,000 r/min, 1 pol-pair, 1 kHz). Paper [19] reports a high speed machine for the turbo application (150,000 r/min, 1 pol-pair, 2.5 kHz). Paper [20] reports a high speed machine for the pump application (20,000 r/min, 4 pol-pair, 1.3 kHz). In order to limit the cost of those above applications, the sensorless motor control schemes are developed [21]-[23]. Although the super-high-speed motor drive does not require a high-precision position feedback, the position information must be robust. The sensorless strategies must be under the risk that the estimation logic falls into a fault, as many non-linear parameters are involved in the observer model. Even though the control algorithm can fast rebuild the estimation [24], however, imagine that the machine is running at 10,000 r/min, the damage will be unacceptable. Hence, a low-cost and robust super-high-speed position measurement is required.

Excellent work has been done to extend the resolver research to the axial filed [25]-[27]. By simply extending the stator-PM VR resolvers to the axial style, an axial topology can be obtained as is shown in Fig.1 (b). Literature [28]-[29] proposed applying printed circuit boards (PCB) winding for VR resolver, instead of the coils winding. The concept is excellent, as the coils assembly is usually a troubling process, the PCB winding will be convenient in the original equipment manufacturer (OEM) factories. But the convex PCB is fragile and costly. By combining the axial resolver structure and the PCB winding skill, the obtained feature is welcome that the winding coils can be laid on a surface, thus the cheap and reliable common PCB can be applied instead of the coils. However, the convex top surface of the rotor is complicated for machining and the entire axial length is long.

This paper improves this axial topology and proposes a compact slotless structure as is shown in Fig.2. By removing the stator teeth and the convex rotor top, the resolver becomes much shorter. Unlike the above VR resolvers, the root novelty of the proposed resolver is that it does not work on the basis of the variable air-gap length. The variable reluctance is realized by the leaf-style rotor swiping through the stator surface. With respect to the turbo, pump and compressor applications, the open-loop launching is a common strategy as the start-up load is light, hence, the high-frequency injection-based low-speed position measurement is not necessary. With this feature, the excitation circuit is rid of from the winding PCB, so the SIN/COS windings can have more space for their circuit, building higher signals. The convex rotor top is replaced by the leaf-style rotor sheet, which is shorter and lighter. For more information on the position measurement at zero- and low-speeds, please refer to paper [14].

In this paper, the axial slotless stator-PM resolver with a leaf-style rotor sheet is proposed and analyzed with two examples, i.e. a 4-X (16 coils, 4 poles) resolver and a 5-X (12 coils, 5 poles) resolver. To validate the mathematical analysis and FEA results, the two examples are prototyped and tested by the experiments.

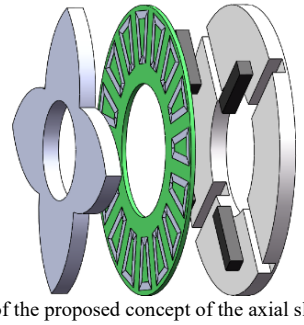

Fig. 2 The structure of the proposed concept of the axial slotless VR resolver.

II. Structure and Analysis

A variable reluctance resolver is a special form of multipole resolver which applies varying magnetoresistance to modulate electrical signals. The resolver in this paper can be considered as a special stator-PM generator, in which a phase shift exists between the two-phase signals, i.e. the SIN/COS signals, which can be used to calculate the rotor angular position.

A. Design with Even Number of Rotor Poles

As an example of the resolver with an even number of salient poles, Fig. 4 illustrates a 16-coil/4-pole VR resolver with two pairs of magnetic poles.

1) *Basic structure*

Fig.2 shows the exploded view of the 16-coil/4-pole VR resolver, Fig. 3(a) illustrates the stator structure, in which the PCB is removed and the winding is sketched for illustration. The rotor part of the resolver is presented in Fig. 3(b), which is a leaf-type sheet. The rotor contour shape is designed to be composed of sinusoidal arcs. For an abstracted linear model, the rotor contour should be exactly sinusoidal. However, consider the actual circular layout, the square coil model becomes a trapezoidal shape, then the rotor contour should change to the presented leaf-style accordingly. Consider the

This article has been accepted for publication in a future issue of this journal, but has not been fully edited. Content may change prior to final publication. Citation information: DOI 10.1109/TIE.2021.3090704, IEEE Transactions on Industrial Electronics

core saturation, edge effect, and structure strength, the contour design cannot be exactly conducted by the analytical method. Several attempts of shape designs are modeled and simulated by the finite element analysis (FEA), with comparisons, the rotor contour used in this paper is enough to verify the practicability of the proposed concept. Fig. 3(c) shows the side view of the entire resolver. Fig. 4 shows the winding distribution of the resolver. In the resolver stator, the four magnets construct two magnetic pole-pairs. One leaf pole of the rotor corresponds to one magnetic pole and sweeps through four stator coils during one electrical period. Thus, the four stator coils can cover 360° elec. To realize the two-phase orthogonal output with a 90° elec. phase shift with respect to one another, the four SIN and COS coils should be located on a quarter circle of the stator surface. This four-coils structure repeats four times along the circumference, forming the stator, with bridges connecting them.

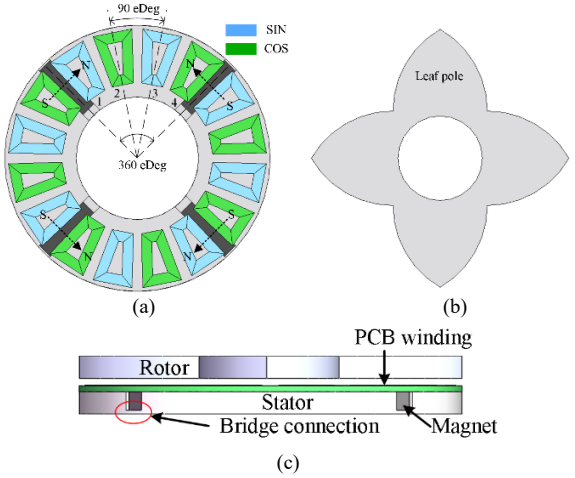

Fig. 3 A typical configuration of the proposed 4-X resolver. (a) The resolver stator. (b) The leaf shape rotor. (c) Side view of the resolver.

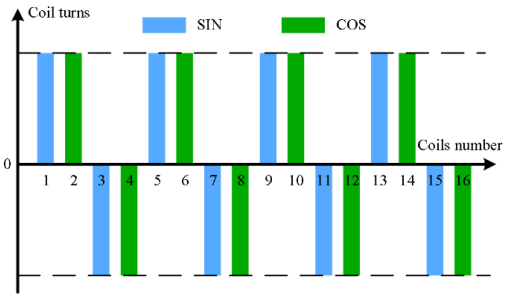

Fig. 4 Winding distribution of the proposed 4-X resolver, 20 turns per coil.

2) *SIN/COS Back-EMFs*

The back-EMF in the SIN winding is analyzed as an example by using the equation (1), and the same thing is happening in the COS winding.

$$E_{\sin}(\theta_r, t) = E_m \sin(p_r \theta_r) \tag{1}$$

In equation (1), θ_r is the rotor angular position, p_r is the rotor pole number. When the rotor leaf pole spins through the four stator coils, the PM flux linkages of the four coils change, inducing alternating back-EMFs (motional back-EMFs). Fig.5 (a) shows the flux linkages in the windings. The SIN and COS flux linkage waves have the same amplitude, but opposite offsets, due to the opposite wiring directions.

E_m in equation (1) is defined as:

$$E_m = p_r \omega_r \varphi_m \tag{2}$$

where φ_m is the PM flux linkage amplitude, ω_r is the mechanical angular speed.

Fig. 5(b) illustrates the orthogonal back-EMFs. The offsets in Fig. 5(a) are removed, as the EMF is the derivative of the flux linkage. Two-phase back-EMFs are two orthogonal sinusoidal voltage signals, which can be converted to calculate the rotor angular position directly by a phase lock loop (PLL).

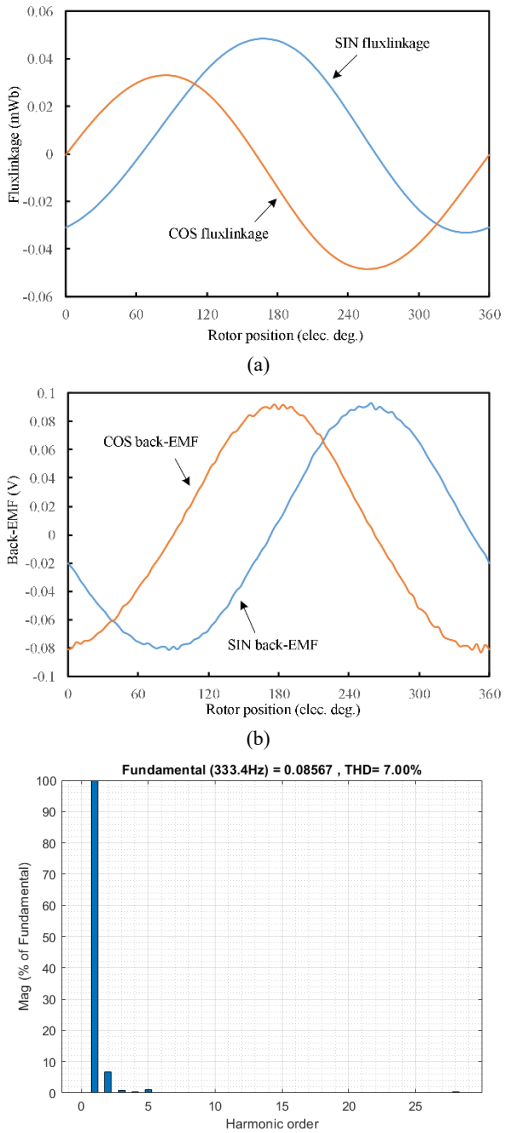

Fig. 5 FEA results of the 4-X resolver. (a) The flux linkages in the windings. (b) The back-EMFs. (c) FFT analysis of the COS back-EMF.

The THD of the COS signal is analyzed by the (fast fourier transform) FFT, there is an obvious 2nd-order component existing in the spectrum. This is because the saturation imbalance occurs on the single-side in each cycle. This phenomenon can be observed in the experimental result, Fig. 14-15.

B. Design with Odd Number of Rotor Poles

In the industrial application, the number of resolvers' rotor

This article has been accepted for publication in a future issue of this journal, but has not been fully edited. Content may change prior to final publication. Citation information: DOI 10.1109/TIE.2021.3090704, IEEE Transactions on Industrial Electronics

salient poles is usually same as the corresponding machine's pole-pair number. High-speed motors are sometimes designed with an odd number of rotor poles [30], therefore the resolver with odd number of poles is also needed. The resolver with odd poles cannot, like the one with even poles, use the intuitive winding distribution scheme. To fully demonstrate the availability of the proposed concept, two resolvers with even or odd poles are discussed respectively in this paper.

As an example of the resolver with odd number of salient poles, Fig.6 illustrates the exploded view of a 5-X VR resolver with the compact slotless structure.

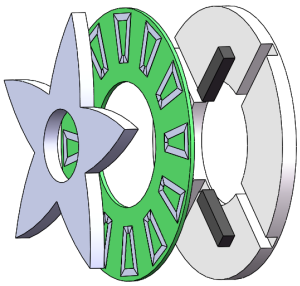

Fig. 6 A 5-X resolver with the slotless structure.

1) *Issue of the Poles Mismatch*

According to the previous plan, one leaf blade corresponds to one magnetic pole, however, when the leaf number is odd, this configuration cannot be implemented. As is illustrated in Fig. 7, the magnetic poles number cannot match the rotor salient pole number. The polarity of the magnet in the red circle cannot be defined. The magnetic poles must come in pairs, thus they can never be with odd numbers. In this paper, this problem is solved by the field modulation concept, taking the 5-X VR resolver as an example.

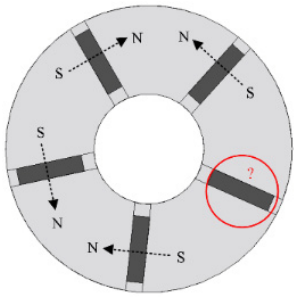

Fig. 7 Magnets distribution with the scheme of the above 4-X resolver.

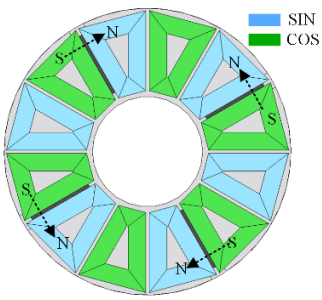

(a)

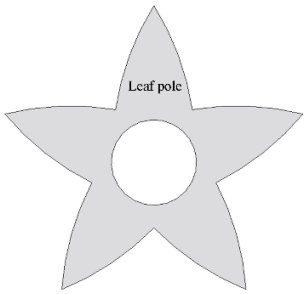

(b)

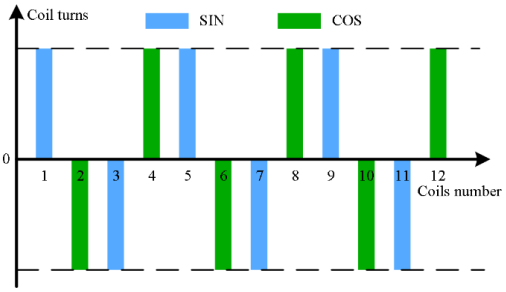

(c)

Fig. 8 A configuration of the proposed 5-X resolver. (a) The resolver stator. (b) The leaf shape rotor. (c) Winding distribution, 32 turns per coil.

2) *Field modulation solution*

The field modulation concept is a novel category of the machine design philosophy [31]-[33] that can coordinate the field components with different pole-pairs. The applicable solution is explained with this 5-X resolver scheme. To explain the concept in a simple way, only fundamental component is considered. Take the signal at position θ_0 as an example, the magneto-motive force (MMF) and permeance are expressed as:

$$F_{PM}(\theta_0) = F_{PM0}\sin(p_{PM}\theta_0) \tag{3}$$

$$\lambda(\theta_0,\theta_r) = \frac{\lambda_{\max}-\lambda_{\min}}{2}\cos\left[p_r(\theta_0-\theta_r)\right] + \frac{\lambda_{\max}+\lambda_{\min}}{2} \tag{4}$$

where θ_0 is the position at the circumference ordinate, F_{PM0} is the maximum amplitude of the MMF, $\lambda_{\max}$ and $\lambda_{\min}$ are the peak values of the airgap permeance. The p_{PM} is magnetic pole-pair number. The field modulation effect produces the flux linkage at θ_0 by the MMF multiplying/modulating the permeance,

$$\begin{aligned}\phi_{PM}(\theta_0,\theta_r) &= NF_{PM}(\theta_0)\lambda(\theta_0,\theta_r)\\ &= \frac{\lambda_{\max}-\lambda_{\min}}{2}NF_{PM0}\cos\left[p_r(\theta_0-\theta_r)\right]\sin(p_{PM}\theta_0)\\ &+ \frac{\lambda_{\max}+\lambda_{\min}}{2}NF_{PM0}\sin(p_{PM}\theta_0)\end{aligned} \tag{5}$$

where N is the number of turns (SIN/COS coils). The modulated motional back-EMFs can be obtained by using the derivative of flux linkage with respect to time.

$$\begin{aligned}E(\theta_0,\theta_r) &= \frac{d\phi_{PM}(\theta_0,\theta_r)}{dt}\\ &= NF_{PM0}\omega_r p_r\frac{\lambda_{\max}-\lambda_{\min}}{2}\sin\left[p_r(\theta_0-\theta_r)\right]\sin(p_{PM}\theta_0)\\ &= E_{PM0}\cos\left[(p_r-p_{PM})\left(\theta_0-\frac{\omega_r p_r}{p_r-p_{PM}}t\right)\right]-\\ &\quad E_{PM0}\cos\left[(p_r+p_{PM})\left(\theta_0-\frac{\omega_r p_r}{p_r+p_{PM}}t\right)\right]\end{aligned} \tag{6}$$

In this case, rotor leaf blade number p_r = 5, magnetic pole-pair number p_{PM} = 2. Fig. 9 is a concise diagram showing the magnetic filed, permeance waveform and winding arrangement.

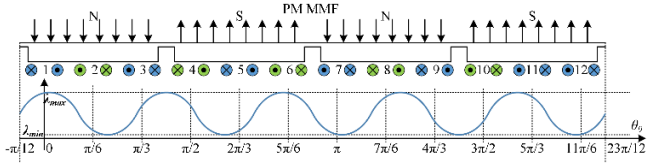

Fig. 9 The concise diagram of field modulation analysis.

By assuming that the permeance waveform is a carrier wave, the MMF can be perceived as a modulation wave. In equation (6), the field modulation effect generates the two components, which can be recognized by the stator windings.

3) *Signal Analysis*

Referring to Fig. 9, the MMF is constant F_{PM} for coils #1, 2, 3, 7, 8, 9, and constant -F_{PM} for coils #4, 5, 6, 10, 11, 12. The flux linkage of coils #1, 2, 3, 7, 8, 9 is expressed as:

$$\phi_{PM}(\theta_0,t)=NF_{PM}\times\left\{\frac{\lambda_{\max}-\lambda_{\min}}{2}\cos\left[p_r(\theta_0-\theta_r)\right]+\frac{\lambda_{\max}+\lambda_{\min}}{2}\right\} \quad (7)$$

The flux linkage expression of the last six is similar, but with a negative sign. The induced SIN/COS flux linkage of the winding is a sum of the six SIN/COS coils:

$$\begin{aligned}\phi_{SIN}(t)&=\phi_{\#1}+\phi_{\#3}+\phi_{\#5}+\phi_{\#7}+\phi_{\#9}+\phi_{\#11}\\&=\phi_{PM}(0,t)-\phi_{PM}\left(\frac{\pi}{3},t\right)-\phi_{PM}\left(\frac{2\pi}{3},t\right)-\phi_{PM}(\pi,t)\\&\quad+\phi_{PM}\left(\frac{4\pi}{3},t\right)+\phi_{PM}\left(\frac{5\pi}{3},t\right)\end{aligned} \quad (8)$$

$$\begin{aligned}\phi_{COS}(t)&=\phi_{\#2}+\phi_{\#4}+\phi_{\#6}+\phi_{\#8}+\phi_{\#10}+\phi_{\#12}\\&=-\phi_{PM}\left(\frac{\pi}{6},t\right)-\phi_{PM}\left(\frac{\pi}{2},t\right)+\phi_{PM}\left(\frac{5\pi}{6},t\right)\\&\quad+\phi_{PM}\left(\frac{7\pi}{6},t\right)+\phi_{PM}\left(\frac{3\pi}{2},t\right)-\phi_{PM}\left(\frac{11\pi}{6},t\right)\end{aligned} \quad (9)$$

The induced back-EMF is the derivative of the flux linkage with respect to time. Therefore, the SIN/COS signals are obtained as:

$$E_{\sin}(t)=\frac{d\phi_{\sin}(t)}{dt}=\sqrt{2}NF_{PM}\omega_r p_r(\lambda_{\max}-\lambda_{\min})\times\left\{\begin{aligned}&-\sin(p_r\theta_r)+\sin\left[p_r\left(\theta_r-\frac{\pi}{3}\right)\right]+\sin\left[p_r\left(\theta_r-\frac{2\pi}{3}\right)\right]\\&+\sin\left[p_r(\theta_r-\pi)\right]-\sin\left[p_r\left(\theta_r-\frac{4\pi}{3}\right)\right]-\sin\left[p_r\left(\theta_r-\frac{5\pi}{3}\right)\right]\end{aligned}\right\} \quad (10)$$

$$E_{\cos}(t)=\frac{d\phi_{\cos}(t)}{dt}=\sqrt{2}NF_{PM}\omega_r p_r(\lambda_{\max}-\lambda_{\min})\times\left\{\begin{aligned}&\sin\left(p_r\left(\theta_r-\frac{\pi}{6}\right)\right)+\sin\left[p_r\left(\theta_r-\frac{\pi}{2}\right)\right]-\sin\left[p_r\left(\theta_r-\frac{5\pi}{6}\right)\right]\\&-\sin\left[p_r\left(\theta_r-\frac{7\pi}{6}\right)\right]-\sin\left[p_r\left(\theta_r-\frac{3\pi}{2}\right)\right]+\sin\left[p_r\left(\theta_r-\frac{11\pi}{6}\right)\right]\end{aligned}\right\} \quad (11)$$

With p_r = 5, the equations (10) and (11) are shorted as:

$$\begin{cases}E_{\sin}(t)=E_{PM0}\sin\left(5\omega_r t+\frac{2\pi}{3}\right)\\E_{\cos}(t)=E_{PM0}\sin\left(5\omega_r t+\frac{7\pi}{6}\right)\end{cases} \quad (12)$$

where $E_{PM0}=4\sqrt{2}NF_{PM}\omega_r p_r(\lambda_{\max}-\lambda_{\min})$.

The proposed resolver model is simulated by FEA, and data is figured in Fig. 10. Fig. 10(a) shows the flux linkage at 5,000 r/min. Fig. 10(b) displays the voltage signals (back-EMFs) E_{SIN} and E_{COS}, which are motional back-EMFs, induced by magnetic field. They are apparently two-phase sinusoidal waveforms with π/2 (90° elec.) phase shift with respect to each other, and exhibit good sine quality, agreeing well to the qualitative analysis in equation (12).

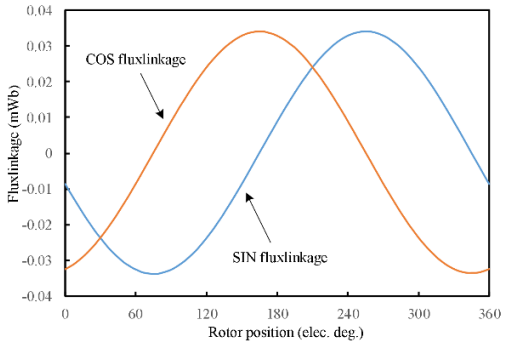

(a)

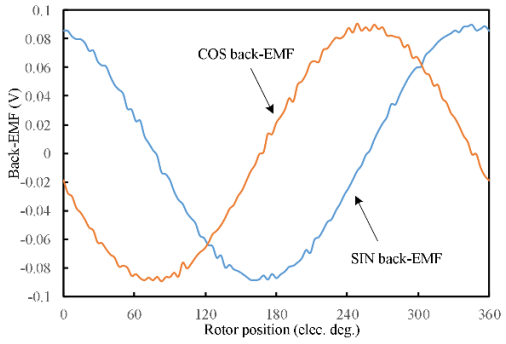

(b)

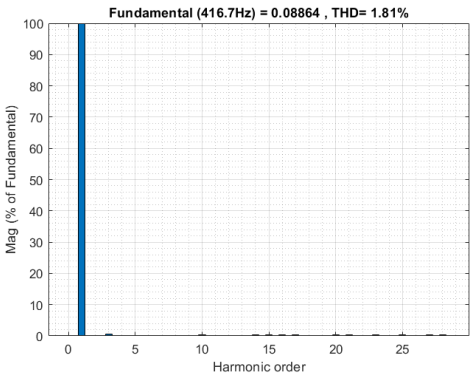

(c)

Fig. 10 FEA results of the 5-X resolver, at 5,000 r/min. (a) The flux linkages in the windings. (b) The back-EMFs. (c) FFT analysis of the COS back-EMF.

With FFT calculation, the signal THD is 1.81%, which is much less than that of the proposed 4-X example. This is because there is no any DC offset in the flux, Fig. 10(a), the saturation effect thus does not affect the signal shape.

III. Signal Processing Scheme

The SIN/COS signals of the resolver are preprocessed by the

amplifier circuit, regulating the signals with the same amplitude and limiting the signals in the range of 0-3 V. The DSP (analog to digital conversion) ADC module then samples the signals. The rotor angular position can be calculated by a normalizer module and a phase-locked loop (PLL) module. Fig. 11 shows the decoding strategy.

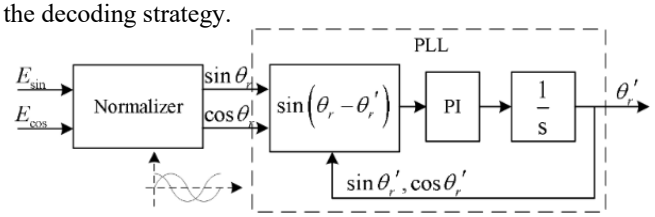

Fig. 11 The rotor angular position calculation strategy.

The signals of the commercial resolvers can be processed by the decoding ICs (e.g. AD2S1210, AU6802) and acquired by a motor controller. For the proposed resolver, there is no need for a special IC, only a common amplifier-composed circuit is required, then a regular processer can extract the angular position directly with only a few microseconds.

IV. Experiment Validation

The two resolvers are prototyped and compared with the commercial resolvers with their corresponding polar pairs.

As the resolvers are prototyped by handwork in the lab, the airgap, stator core and rotor are thick for easy assembling. The windings are made by a 0.8 mm thickness PCB with 4 layers. For industrial manufactures, the thicknesses of the components can be appropriately reduced, the PCB layers can be improved, and the axial size of the resolver can thus further reduce, then the thinner resolver and lower cost can be obtained.

To validate the function of the proposed resolver system, an experimental setup is established as shown in Fig. 12. The commercial resolver (benchmark) and the proposed prototype are back-to-back gathered on the same shaft, driven by a DC brush motor. Limited by the mechanical installation, the system can stably support testing up to 10,000 r/min. The commercial resolver requires a commercial decoding chip (AD2S1210) on the decoding board.

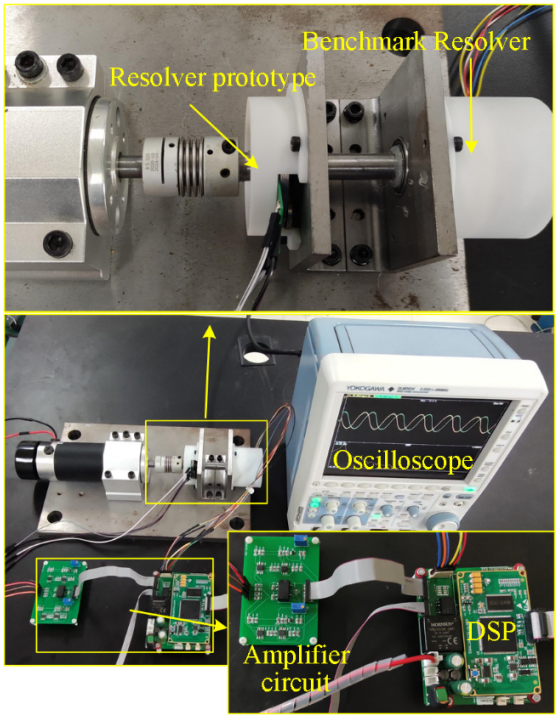

Fig. 12 Construction of the experimental setup.

There are three digital-to-analog channels (DACs) on the DSP, two channels display the decoded angular position, by the proposed resolver and the commercial resolver respectively. And the third channel is to display the measurement error.

There is an AD2S1210 based decoding circuit mounted with the DSP (TMS320F28379D), which can acquire the shaft angular position from the AD2S1210. Meanwhile, the amplifier circuit processes the differential SIN/COS signals, and provides regulated signals to the DSP ADC channels for the decoding. By this way, the DSP can acquire the shaft angular position from the two resolvers synchronously, and calculate the error.

A. Example I: 4-X resolver

Table I compares the dimension parameters of the proposed 4-X VR resolver and a Tamakava 4-X VR resolver (TS2225N 1974E102).

Fig. 13(a) shows the prototype of the proposed 4-X resolver, Fig. 13(b) compares the prototype and the corresponding commercial resolver.

TABLE I
Dimension comparison of the proposed 4-X and typical VR resolver

Parameters	Proposed	Benchmark
Stator coils/rotor poles	16/4	/
Stator outer diameters (mm)	52	52
Axial length (mm)	8.3	16
Air-gap length (mm)	1.2	1.0 (min)*
Magnet amount (g)	2.7	-

* measured dimension, not precise value.

This article has been accepted for publication in a future issue of this journal, but has not been fully edited. Content may change prior to final publication. Citation information: DOI 10.1109/TIE.2021.3090704, IEEE Transactions on Industrial Electronics

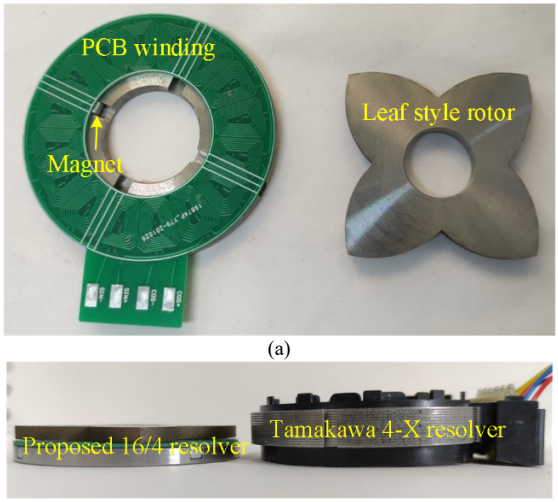

Fig. 13 The proposed 4-X prototype. (a) The proposed resolver components. (b) Comparison with the Tamakava resolver.

The SIN/COS windings provide two-phase orthogonal PM back-EMFs, as is shown in Fig. 14, identical to the FEA results in Fig. 5(b). The amplitude of the SIN/COS PM back-EMFs can be stably detected by the analog circuit. As is shown in the top zoom window, at 5,000 r/min, the phase shift between the back-EMFs is 0.75 ms, i.e., 90° elec. Due to the improper PCB layout design, the SIN analog signal amplitude is lower than the COS signal. In the experimental validation, this imbalance can be compensated by the amplifier circuit. For the further real application, the SIN and COS layout design on the PCB must be strictly symmetrical to create same signal amplitudes.

In the bottom zoom window, the FFT frequency spectrogram of COS signal is shown. The 310 Hz component is with 63 mV amplitude and the THD is 5.3%. The SIN/COS waveforms are not with perfect sine quality as expected, caused by the eccentric installation and intrinsic unbalanced saturation effect. But the signals can support the position calculation, with some errors though.

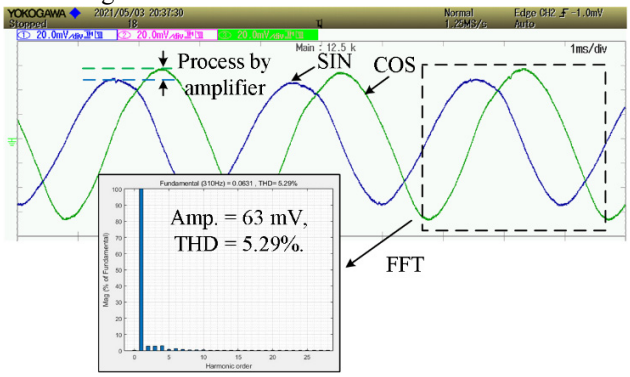

Fig. 14 The raw SIN/COS signals of the proposed 4-X resolver.

After an amplifier circuit processing, the signals in Fig. 14 are modified to signals that can be sampled by ADC of the DSP. Then the digital signal process can calculate the rotor angle.

A four channel oscilloscope is used to present the experimental measurement. Fig. 15 shows the results at 800 r/min, 5,000 r/min, and 10,000 r/min. The channel 1 shows the modified COS signal, which is in the range of 0-3 V. Channel 2 shows the discrepancy between the proposed resolver measurement and the benchmark. Channel 3 shows the benchmark, i.e. the position read from the decoding IC. Channel 4 shows the position extracted from the measured SIN/COS signals.

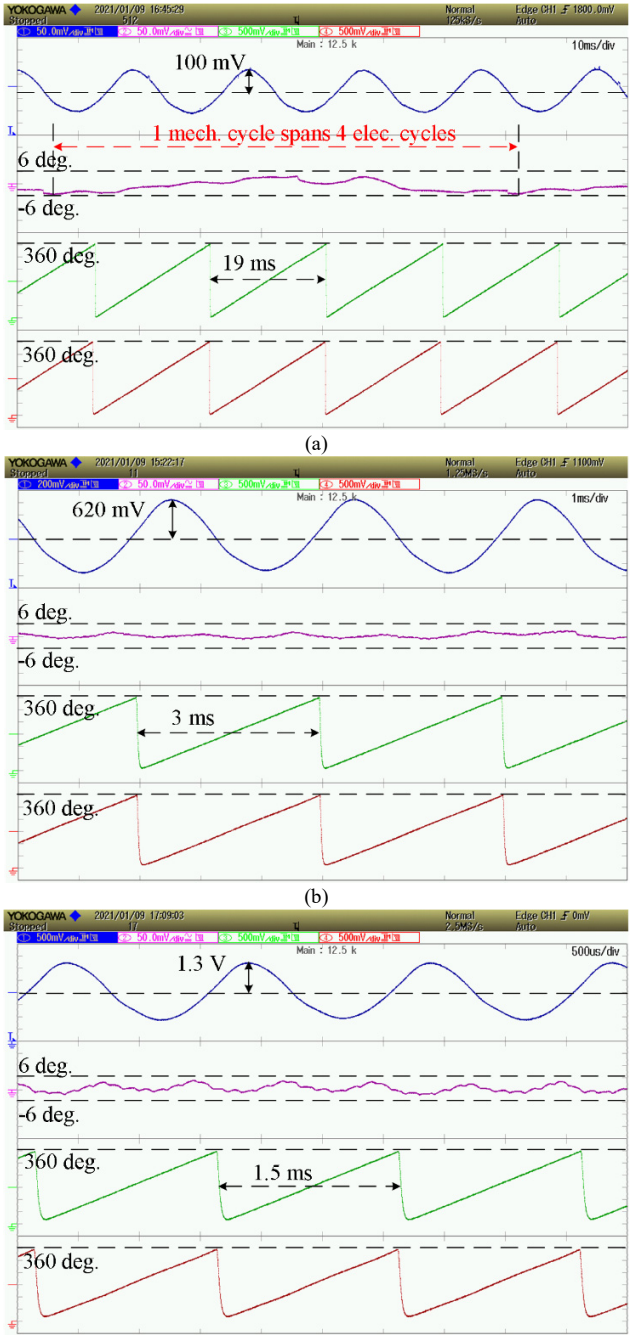

Fig. 15 The position measurement of the 4-X resolver. (CH1: COS signal; CH2: position error; CH3: benchmark; CH4: the proposed measurement.) (a) 800 r/min. (b) 5,000 r/min. (c) 10,000 r/min.

Some conclusions can be extracted from Fig. 15. First, the COS signal amplitude linearly increases with the rotor speed. Second, the measurement error can be limited within 6° elec.

There are some further discussions on the measurement error. The imperfect sine quality of the SIN/COS signals caused by

This article has been accepted for publication in a future issue of this journal, but has not been fully edited. Content may change prior to final publication. Citation information: DOI 10.1109/TIE.2021.3090704, IEEE Transactions on Industrial Electronics

the unbalanced saturation should be responsible for the errors. On the other hand, the mechanical assembling should also be considered. In Fig. 15(a), the heavy error periodically occurs and this period takes four electrical cycles. It is supposed that the rotor surface is not strictly parallel to the stator core surface. This is because the rotor is a 3 mm thick sheet, which is prone to be tilted, especially for the not very tight assembly. At low speeds, this tilt induces the position error happening in every mechanical period, i.e., four electrical periods, Fig. 15(a). At high speeds, with the gyroscopic effect, the tilt could get modified to some extent, less than 3° elec. in Fig. 15(b). But the error increases at very high speeds, less than 5° elec. in Fig. 15(c), as the vibration gets fierce with the unbalanced centrifugal force. Hence, the machining and assembly of the rotor is critical for the proposed axial resolver.

B. Example II: 5-X resolver

Table II compares the dimension parameters of the proposed 5-X VR resolver and a commercial resolver (TS2640N 321E64).

TABLE II
Dimension comparison of the proposed 5-X resovler and typical VR resolver

Parameters	Proposed	Benchmark
Stator coils/rotor poles	12/5	/
Stator outer diameters (mm)	52	52.4
Axial length (mm)	8.3	27.1
Air-gap length (mm)	1.2	0.4 (min)*
Ferrite amount (g)	2.7	-

* measured dimension, not precise value.

Fig. 16(a) shows the proposed 5-X resolver prototype, Fig. 16(b) compares the prototype and a 1-X winding rotor resolver, which is popular in the servo industry. As a benchmark, one cycle position data of the 1-X resolver can be transformed to be with 5 cycles to match the 5-X resolver.

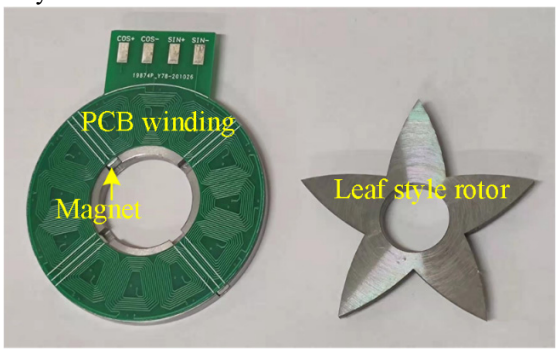

(a)

(b)

Fig. 16 The proposed 5-X prototype. (a) The proposed resolver components. (b) Comparison with the Tamakava resolver.

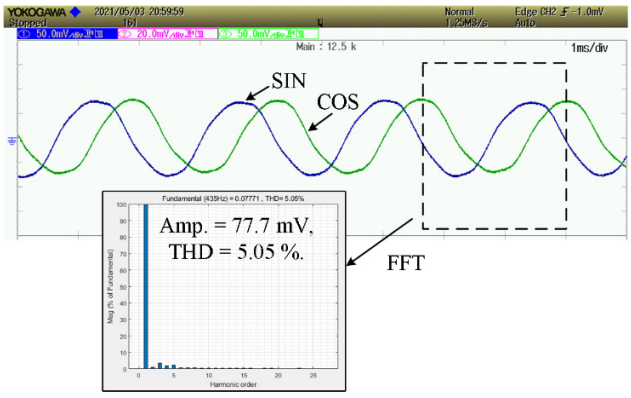

Fig. 17 The raw SIN/COS signals of the proposed 5-X resolver.

The SIN/COS windings provide the two-phase orthogonal PM back-EMFs, the analog signals in Fig. 17, identical to the FEA results in Fig. 10(b). The SIN/COS signals are shown in the top zoom window, at 5,000 r/min, the phase shift between the SIN/COS signals is 0.6 ms, i.e., 90° elec.

In the bottom zoom window, the FFT spectrogram of COS signal is shown. The 435 Hz component is with 77.7 mV amplitude and the THD is 5.05 %. The THD of proposed 5-X resolver is smaller than the 4-X prototype.

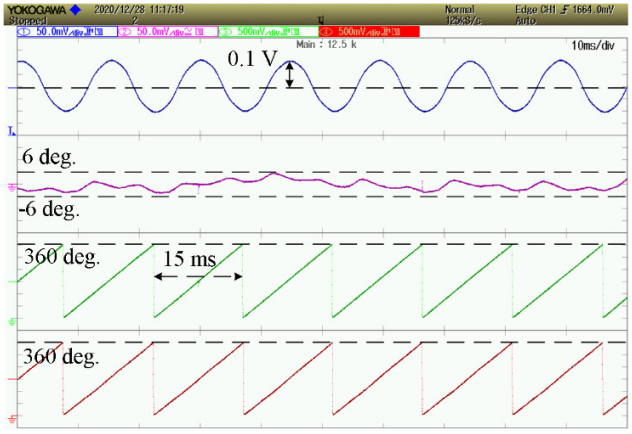

(a)

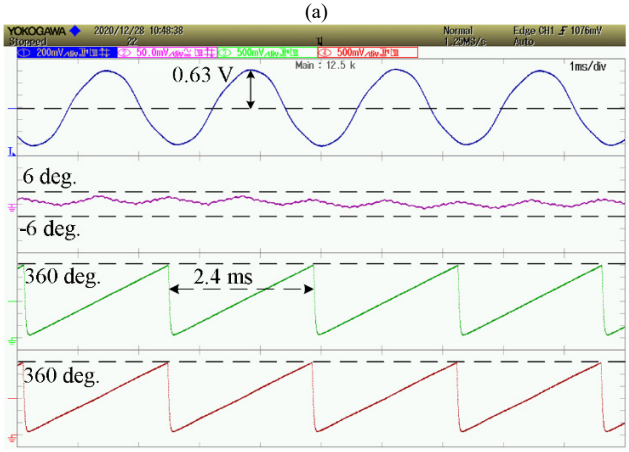

(b)

This article has been accepted for publication in a future issue of this journal, but has not been fully edited. Content may change prior to final publication. Citation information: DOI 10.1109/TIE.2021.3090704, IEEE Transactions on Industrial Electronics

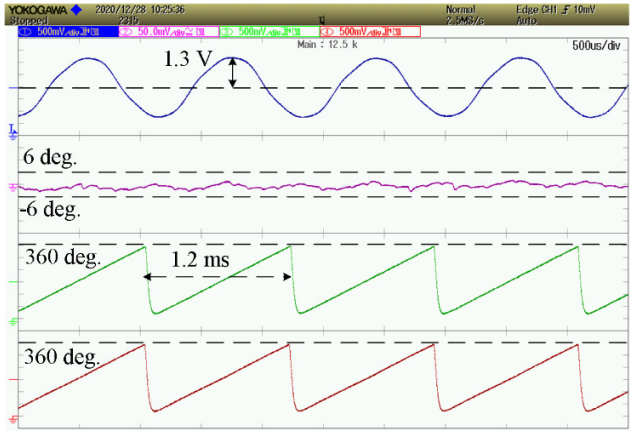

(c)

Fig. 18 The position measurement of the 5-X resolver. (CH1: COS signal; CH2: position error; CH3: benchmark; CH4: the proposed measurement.) (a) 800 r/min. (b) 5,000 r/min. (c) 10,000 r/min.

The experimental result of the 5-X resolver presents similar features to the 4-X resolver, but with a higher accuracy, as the THD of the 5-X resolver signal is better, and the machining of the 5-X rotor is updated. The maximum measurement error at 10,000 r/min is around 3° elec.

C.Practice on the Motor Drive

To practice the proposed resolver, a new 4-X resolver is prototyped and equipped onto a PMSM motor, replacing the original encoder. The parameters of the motor and revolver are listed in Table III.

TABLE III
Parameters of the motor and the equipped 4-X VR resolver

Resolver		Motor	
Stator coils/rotor poles	16/4	Pole-pairs	4
Stator outer diameters (mm)	34	Nominal power (W)	400
Axial length (mm)	8.2	DC bus (V)	350
Air-gap length (mm)	1.2	Max. speed (r/min)	3300
Magnet amount (g)	2.3	Rating torque (Nm)	1.2

The testing rig is shown in Fig. 19, where the 4-X resolver is mounted on the shaft tail of the PMSM motor. The size and cost of this resolver are comparable to the hall sensors. As is stated before, this type of resolver is designed with respect to the pump and turbo applications, a 12-blade propeller is equipped in front of the motor, the load torque increases with the motor speed, reaching around 1 Nm at 3000 r/min. A motor controller with TMS320F28379D is developed to drive the PMSM, as the withstand voltage of the main capacitors is 450 V, the DC bus voltage is limited under 350 V for the safety reason, then the maximum speed the system can reach is around 3300 r/min without the flux weakening. The controller can receive the speed command and upload the actual speed by the CAN bus. The oscilloscope displays the sampled SIN/COS signals and decoded rotor angle via the DSP DAC channels.

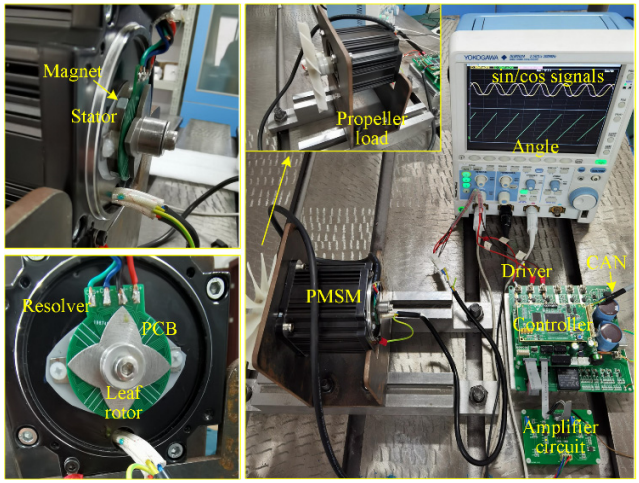

Fig. 19 Practicing the proposed resolver with a PMSM motor.

The DSP28379D has two CPUs, which can run different programs independently. In this project, the CPU1 conducts the main motor control mission with a 10 kHz space vector pulse width modulation (SVPWM). The required angle information is extracted by the CPU2 from a 200 kHz sample of the SIN/COS signals. The CPU1 can grab the rotor angle in each of the PWM switch period. Fig. 20 shows the diagram of the drive system. The raw SIN/COS signals are differential, and the amplitudes are too small for the DSP ADC, hence they cannot be provided to the DSP directly. Fig. 21 shows the raw signals when the motor shaft is passively motored by a hand electric drill at 380 r/min and 1500 r/min respectively. The signal amplitudes are around 20 mV at 380 r/min. As the hand drill cannot hold a constant speed at low-speeds, the waveform shapes are not ideally sinusoidal, but the signals are clean and without unacceptable noises, so it can support for the angle decoding. The hand drill speed is stable at 1500 r/min, then the SIN/COS signals exhibit good sinusoidal shape, the THD is 3.85%, which is even better than the previous FEA result of the 16/4 resolver. Anyway, these signals can well support for the angle decoding. As the amplitude is 82 mV at 1500 r/min, it can be calculated that it can reach 180 mV at 3300 r/min, so the peak-peak value (V_{pp}) is 360 mV. The ADC range is 3 V, and the gain of the amplifier is set to be 15, so the V_{pp} after the amplifier circuit will be 2.7 V, included by the ADC range.

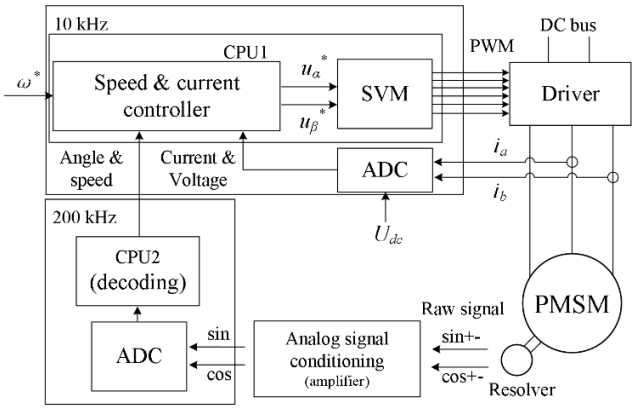

Fig. 20 Diagram of the dual-CPU motor drive system on the basis of the proposed resolver.

This article has been accepted for publication in a future issue of this journal, but has not been fully edited. Content may change prior to final publication. Citation information: DOI 10.1109/TIE.2021.3090704, IEEE Transactions on Industrial Electronics

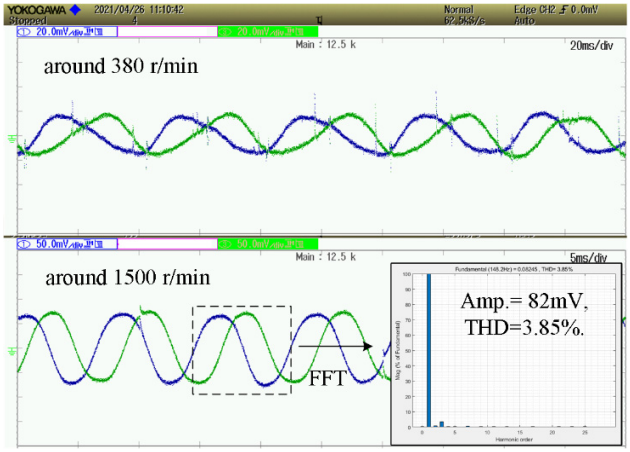

Fig. 21 The raw signals generated by the resolver coils.

After the amplifier circuit, the SIN/COS signals are sampled by the CPU2 per 5 us. By generating the calculation signals via the DAC channels, the phase shift between the sampled signals and the decoded rotor angle can be measured. In Fig. 22(a), the decoded angle starts from the zero-cross point of the sampled SIN signal. Without the driver, the motor phase back-EMF can be synchronously measured with the rotor angle. The zero-cross point of the phase back-EMF is lagging the start of the rotor angle by 109° elec. This delay is due to the installation position of the resolver, and can be compensated in the decoding software. In Fig. 22(b), with a compensation, the rotor angle is shifted by 109° elec. to align with the phase-A back-EMF. This shift compensation is saved in the control program, so this calibration does not need be repeated as long as the resolver is not reinstalled. The SVPWM can be conducted with this home set angular position.

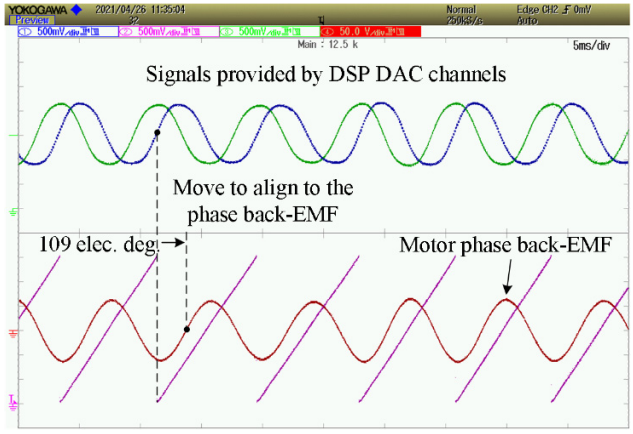

(a)

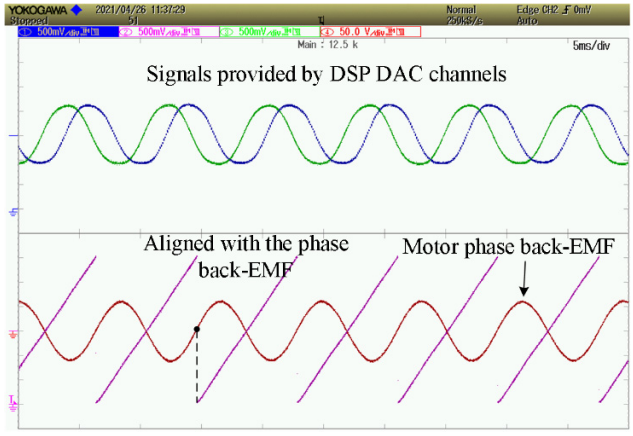

(b)

Fig. 22 Calibration to correct the home set angular position. (a) Raw rotor angle extracted from the SIN/COS signals. (b) The rotor angle shifts by 109° elec. to align with the phase-A back-EMF.

A motor speed control is realized with the angle information, shown in Fig. 23(a). Before the resolver signal is significant, the motor starts by an open-loop startup, during which the propeller load torque is negligible. As long as the angle is available, the motor speed control switches to close loop, and the speed is kept at the idle speed 500 r/min. Then the step response is tested at 3300, 2000, and 1000 r/min respectively. It can be found that the speed stability is better at high-speeds, rather than at low-speeds. This is because the high amplitude signals have better immunity against the sampling noises.

All the above back-EMF signals present clean and clear waveform when the machine is motored by an external driver (the DC brush motor or the electric hand drill). However, when the 10 kHz PWM switching is applied, the 10 kHz noises can be observed in the DAC channels. Although it is not easy to judge that whether the noises are on the ADC or on the DAC channels, the DSP analog system must have been contaminated by the PWM switching in the power stage. Some specific isolation and shield measures should be added to suppress this noises. However, from the other perspective, this proposed angular position measurement is reliable, and can withstand the terrible noises.

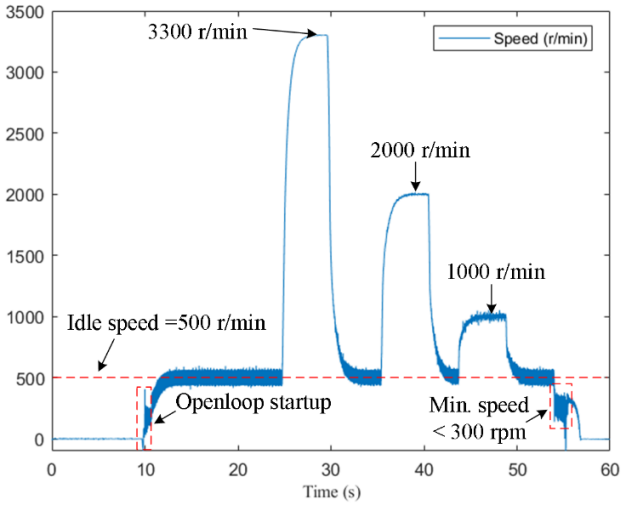

(a)

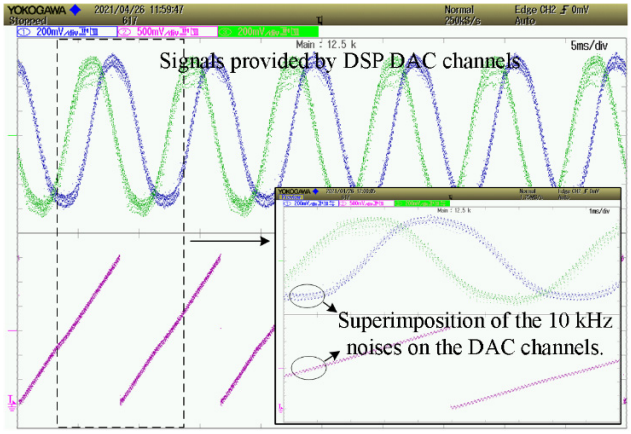

(b)

Fig. 23 Speed control with the proposed resolver. (a) The recorded motor speed during the test. (b) Sampled signals and decoded rotor angle at 1500 r/min.

D. Discussion and Future Work

The above experiments have helped to realize the expected function of the proposed concept, which is the main notion of this paper. There are two imperfections happening in the experiment. First, the SIN signal is lower than the COS signal, which is shown in Fig. 14. This is because there is a difference between SIN and COS winding resistance in PCB circuit. The PCB layout must be redesigned. But this issue can be solved by a proper amplifier gain. Second, the THD of the proposed 5-X resolver signal is better than that of the 4-X prototype, the position error is also less than the latter. The improvement work is discussed and planned below.

The root cause of the poor THD in the 4-X prototype is the DC offset on the flux, Fig. 5(a), the asymmetrical saturation effect damages the sine quality of the signals. Unlike the 4-X prototype, the saturation symmetrically happens on the positive and negative sides of the 5-X flux, Fig. 10(a). A potential method to improve the 4-X performance is to apply the field modulation concept, by which, the winding can be redesigned with several other options. There would be a chance to remove the DC offset by a proper winding distribution. As the space is limited, the related research will be reported in further work.

V. Conclusion

The main contribution of this paper is to extend the concept of stator-PM VR resolver to the axial resolver field. The compact axial VR resolvers with leaf-style rotors are analyzed and developed. In addition to the resolver with even pole-pairs provided by a regular scheme, the odd pole-pairs scheme is proposed based on the principle of magnetic field modulation.

Two prototypes for the proposed 4-X and 5-X VR resolvers with the dedicated measurement and decoding system have been developed. Validated by the experimental results, the expected position measurement function is realized. Moreover, a new 4-X resolver is specially designed for a PMSM, and equipped on the motor, the entire drive system is developed and the speed control on basis of the proposed resolver is validated.

References

[1] L. Z. Sun, “Analysis and improvement on the structure of variable reluctance resolvers,” *IEEE Transactions on Magnetics*, vol. 44, no. 8, pp. 2002–2008, Aug. 2008.

[2] F. Mapelli, D. Tarsitano, and M. Mauri, “Plug-in hybrid electric vehicle: Modeling, prototype realization, and inverter losses reduction analysis,” *IEEE Transactions on Industrial Electronics*, vol. 57, no. 2, pp. 598–607, Feb. 2010.

[3] J. Figueiredo, “Resolver models for manufacturing,” *IEEE Transactions on Industrial Electronics*, vol. 58, no. 8, pp. 3693–3700, Aug. 2011.

[4] R. Alipour-Sarabi, Z. Nasiri-Gheidari, F. Tootoonchian, and H. Oraee, “Analysis of winding configurations and slot-pole combinations in fractional-slots resolvers,” *IEEE Sensors Journal*, vol. 17, no. 14, pp. 4420–4428, Jul. 2017.

[5] R. Alipour-Sarabi, Z. Nasiri-Gheidari, F. Tootoonchian, and H. Oraee, “Improved winding proposal for wound rotor resolver using genetic algorithm and winding function approach,” *IEEE Transactions on Industrial Electronics*, vol. 66, no. 2, pp. 1325–1334, Feb. 2019.

[6] X. Ge, and Z. Q. Zhu, “A novel design of rotor contour for variable reluctance resolver by injecting auxiliary air-gap permeance harmonics,” *IEEE Transactions on Energy Conversion*, vol. 31, no. 1, pp. 345–353, Mar. 2016.

[7] X. Ge, Z. Q. Zhu, R. Ren, and J. T. Chen, “A novel variable reluctance resolver with non-overlapping tooth–coil windings,” *IEEE Transactions on Energy Conversion*, vol. 30, no. 2, pp. 784–794, Mar. 2015.

[8] Analog Devices, Inc. “Variable resolution, 10-bit to 16-bit R/D converter with reference oscillator—AD2S1210” Datasheet, www.analog.com, 2008.

[9] Z. Zhang, F. Ni, Y. Dong, C. Guo, M. Jin, and H. Liu, "A novel absolute magnetic rotary sensor", *IEEE Transactions on Industrial Electronics*, vol. 62, no. 7, pp. 4408-4419, Jul. 2015.

[10] B. Aschenbrenner, and B. G. Zagar, “Analysis and validation of a planar high-frequency contactless absolute inductive position sensor,” *IEEE Transactions on Instrumentation and Measurement*, vol. 64, no. 3, pp. 768–775, Mar. 2015.

[11] J. R. Lunean, “Magnetic structure for synchro and tachometer”, US patent, No. 4659953, Apr. 1987.

[12] Ming Cheng, K. T. Chau and C. C. Chan, "Static characteristics of a new doubly salient permanent magnet motor," *IEEE Transactions on Energy Conversion*, vol. 16, no. 1, pp. 20-25, March 2001.

[13] W. Hua, M. Cheng, Z. Q. Zhu and D. Howe, "Analysis and Optimization of Back EMF Waveform of a Flux-Switching Permanent Magnet Motor," *IEEE Transactions on Energy Conversion*, vol. 23, no. 3, pp. 727-733, Sept. 2008.

[14] L. Sun, J. Taylor, A. D. Callegaro and A. Emadi, "Stator-PM-based variable reluctance resolver with advantage of motional back-EMF," *IEEE Transactions on Industrial Electronics*, vol. 67, no. 11, pp. 9790-9801, Nov. 2020.

[15] L. Sun, Z. Luo, K. Wang, R. Cao and S. Ding, "A Stator-PM resolver with field modulation principle," *IEEE Transactions on Energy Conversion*, doi: 10.1109/TEC.2020.3001655.

[16] L. Sun, J. Taylor, X. Guo, M. Cheng and A. Emadi, "A linear position measurement scheme for long-distance and high-speed applications," *IEEE Transactions on Industrial Electronics*, doi: 10.1109/TIE.2020.2984447.

[17] M. Bahari, A. Davoodi, H. Saneie, F. Tootoonchian and Z. Nasiri-Gheidari, "A New Variable Reluctance PM Resolver," *IEEE Sensors Journal*, vol. 20, no. 1, pp. 135-142, Jan. 2020, doi:10.1109/JSEN.2019.2941554.

[18] N. Uzhegov, A. Smirnov, C. H. Park, J. H. Ahn, J. Heikkinen and J. Pyrhönen, "Design aspects of high-speed electrical machines with active magnetic bearings for compressor applications," *IEEE Transactions on Industrial Electronics*, vol. 64, no. 11, pp. 8427-8436, Nov. 2017.

[19] M. Lim, J. Kim, Y. Hwang and J. Hong, "Design of an ultra-high-speed permanent-magnet motor for an electric turbocharger considering speed response characteristics," *IEEE/ASME Transactions on Mechatronics*, vol. 22, no. 2, pp. 774-784, April 2017.

[20] A. Al-Timimy et al., "Design and losses analysis of a high power density machine for flooded pump applications," in IEEE Transactions on Industry Applications, vol. 54, no. 4, pp. 3260-3270, July-Aug. 2018, doi: 10.1109/TIA.2018.2821623.

[21] G. Wang, D. Xiao, G. Zhang, C. Li, X. Zhang and D. Xu, "Sensorless control scheme of IPMSMs using HF orthogonal square-wave voltage

injection into a stationary reference frame," *IEEE Transactions on Power Electronics*, vol. 34, no. 3, pp. 2573-2584, March 2019.
[22] L. Sun, S. Nalakath, A. D. Callegaro and A. Emadi, "Investigation of a practical convex-optimization-based sensorless scheme for IPMSM drives," *IEEE Transactions on Power Electronics*, vol. 34, no. 12, pp. 12437-12452, Dec. 2019.
[23] G. Wang, D. Xiao, N. Zhao, X. Zhang, W. Wang and D. Xu, "Low-frequency pulse voltage injection scheme-based sensorless control of IPMSM drives for audible noise reduction," *IEEE Transactions on Industrial Electronics*, vol. 64, no. 11, pp. 8415-8426, Nov. 2017.
[24] F. Peng, J. Ye, A. Emadi and Y. Huang, "Position sensorless control of switched reluctance motor drives based on numerical method," *IEEE Transactions on Industry Applications*, vol. 53, no. 3, pp. 2159-2168, May-June 2017.
[25] Z. Nasiri-Gheidari, "Design, analysis, and prototyping of a new wound-rotor axial flux brushless resolver," *IEEE Transactions on Energy Conversion*, vol. 32, no. 1, pp. 276-283, March 2017.
[26] H. Saneie, Z. Nasiri-Gheidari and F. Tootoonchian, "Design-Oriented Modelling of Axial-Flux Variable-Reluctance Resolver Based on Magnetic Equivalent Circuits and Schwarz–Christoffel Mapping," *IEEE Transactions on Industrial Electronics*, vol. 65, no. 5, pp. 4322-4330, May 2018.
[27] R. Alipour-Sarabi, Z. Nasiri-Gheidari, F. Tootoonchian and H. Oraee, "Improved winding proposal for wound rotor resolver using genetic algorithm and winding function approach," *IEEE Transactions on Industrial Electronics*, vol. 66, no. 2, pp. 1325-1334, Feb. 2019.
[28] S. Park and K. Kim, "Study on the Optimal Design of a Novel Slotless Resolver by FEM," *IEEE Transactions on Magnetics*, vol. 50, no. 11, pp. 1-4, Nov. 2014, Art no. 8001904, doi: 10.1109/TMAG.2014.2318795.
[29] W. Y. Lee, B. C. NA, "Slotless resolver, method for manufacturing same, and wiring tool used therefor," Daesung Electric Co., Ltd., Patent, *WO*, WO2013/118966A1, https://patents.google.com/patent/WO2013118966A1/en
[30] N. Fernando, P. Arumugam and C. Gerada, "Design of a stator for a high-speed turbo-generator with fixed permanent magnet rotor radius and volt–ampere constraints," *IEEE Transactions on Energy Conversion*, vol. 33, no. 3, pp. 1311-1320, Sept. 2018.
[31] M. Cheng, P. Han, and W. Hua, "General airgap field modulation theory for electrical machines," *IEEE Transactions on Industrial Electronics*, vol. 64, no. 8, pp. 6063-6074, Aug. 2017.
[32] H. Wen, M. Cheng, "Unified analysis of induction machine and synchronous machine based on the general airgap field modulation theory," *IEEE Transactions on Industrial Electronics*, vol. 66, no. 12, pp. 9205-9216, Dec. 2019.
[33] M. Cheng, H. Wen, P. Han, "Analysis of airgap field modulation principle of simple salient poles," *IEEE Transactions on Industrial Electronics*, vol. 66, no. 4, pp. 2628-2638, Apr. 2019.

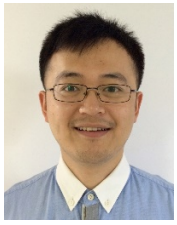

Le Sun (IEEE S'15–M'17) received the Ph.D. degree in electrical engineering from the School of Electrical Engineering, Southeast University, Nanjing, China, in 2016. From 2016 to 2018, he was working as a Postdoctoral researcher in McMaster Automotive Resource Centre, McMaster University, ON, Canada.

Since 2019, he has been with Nanjing University of Science and Technology (NUST), Nanjing, China, where he is an Associate Professor of the department of electrical engineering, and a joint research fellow of the School of Mechanical Engineering. His teaching and research interest includes design, and control of PM machines for servo systems, and electric vehicles.

Zhejun Luo（IEEE S'20） received the B.Sc. degree in electrical engineering from Southeast University, Nanjing, China, in 2018. She is currently working toward the M.Sc. degree in electrical engineering at Anhui University.

Her research interests in permanent-magnet motors, including the machine and drive system.

Jun Hang（S'12-M'16）received the B.Sc. and M.Sc. degrees in electrical engineering from Anhui University of Science & Technology, Huainan, China, in 2008 and 2011, respectively, and the Ph.D. degree in electrical engineering from Southeast University, Nanjing, China, in 2016. From April 2015 to July 2015, He was a joint Ph. D. student with the Department of Energy Technology, Aalborg University, Denmark.

Since 2016, he has been with Anhui University, Hefei, China, where he is currently an Associate Professor in the School of Electrical Engineering and Automation. His current research interests include condition monitoring and fault diagnosis. In recent years, he has authored and co-authored over 40 technical papers. Dr. Hang received the 1st Prize of 2016 Student Thesis Contest (PhD Category), IEEE Industry Applications Society.

Shichuan Ding（S'08-M'12） received the B.Sc. degree in automation from Anhui University, Hefei, China, in 2001 and the M.Sc. degree from USTC, Hefei, China, in 2006, and the Ph.D. degree in electrical engineering from Southeast University, Nanjing, China, in 2018.

Since 2001, he has been with Anhui University, where he is currently a Professor. He has been a Research Scholar with WEMPEC in University of Wisconsin Madison from April 2015 to April 2016. His research interests include electrical machine drive, electrical machine fault diagnosis and fault tolerant control, power electronics applications and energy management in EVs, in industrial application and in power system. In recent years, he has authored and co-authored over 40 technical papers.

Wei Wang (S'10-M'14-SM'19) was born in Jiangsu, China. He received the B.Sc. degree in electrical engineering from Nanjing University of Science & Technology, Nanjing, China, in 2008, and the Ph.D. degree in electrical engineering from Southeast University, Nanjing, China, in 2014, respectively.

Since 2014, he has been with Southeast University, where he is currently an associate professor in the School of Electrical Engineering. From October 2011 to October 2012, he got the scholarship from China Scholarship Council and was a joint Ph. D student with University of Lille 1, Lille, France. He is the author or coauthor of more than 30 technical papers. His research interests include motor drives and electrified transport.